FR8701500

GANIL

THE LISE SPECTROMETER AT GANIL

M.G. SAINT-LAURENT

GANIL, BP. 5027, 14021 Caen-Cedex, France

Talk given at the XI International Conference on Electromagnetic Isotope Separators and Techniques related to their applications.
LOS ALAMOS, New Mexico, August 18-22, 1986.

GANIL P. 86-18

THE LISE SPECTROMETER AT GANIL

M.G. SAINT-LAURENT

GANIL, BP. 5027, 14021 CAEN-CEDEX, France

ABSTRACT : The doubly achromatic spectrometer LISE is available at the french national heavy ion accelerator GANIL. Experimental results, obtained in radioactive beam production and search for new exotic nuclei are briefly reported.

I - INTRODUCTION

The LISE* spectrometer, installed at GANIL, was designed for the production of secondary beams with good optical properties [1]. Fully stripped or hydrogen and helium like heavy ion species of great interest in atomic physics can be produced with LISE. But this line is also very useful for the research of nuclei far from stability.

Experimental set-up and improvements are described in section II. In section III, I shall explain the production of secondary beams and the results obtained near the proton drip line above Z=20. Finally, a chart of nuclides with all the exotic nuclide results, obtained at GANIL, is presented.

II - EXPERIMENTAL SET-UP

II.1 - General features of the LISE spectrometer

LISE is a doubly achromatic spectrometer (fig. 1), in angle as well as in position ; this ensures, at first order, a constant flight-path length ($\Delta l/l = 10^{-3}$ l=18 m for the total acceptance ± 2.5%) between the production target and the detector position ; thus the measurement of the time of flight is an important parameter, in the particle identification.

For the purpose of this conference, I shall describe briefly LISE and resume its main characteristics. More details can be found in ref. [1,2,3].

The primary beam is focused onto the production target T using 4 quadrupoles q_1 to q_4. Up to ten different targets can be mounted on a water-cooled copper wheel. Easy target change is available by remote control of the wheel position, without entering in the experimental aera.

* LISE (Ligne d'Ions Super Epluchés) means Highly Stripped Ion Beams.

Secondary products emitted at zero degree are analysed or dispersed as A/Z, by the first section of the line composed of the first dipole D1 and the quadrupoles lenses Q_1 to Q_4. Remote controlled variable aperture slits are located at the intermediate dispersive focal plane : they allow to limit the $B\rho$ acceptance of the line. An additional stripper foil, or an energy degrader or a thin position-sensitive detector can be placed behind these slits.

The second dipole D2 asociated with the quadrupole lenses Q_5-Q_6 compensates the dispersion of the firt section. Such a system is doubly achromatic, in angle as well as in position. The quadrupole lenses Q_7 to Q_{10} are used to focus the products in the final focal point of the experimental aera where are located the detectors.

In order to protect from radiations the sensitive detectors, the first dipole D1 is a largely dimensioned C-type magnet which allows primary beam catching far away from the transmitted beam. A concrete shielded wall is separating the physics detectors from the primary beam catcher. Any unchecked change of the dipole magnetic field is detected by pick-up coils and instantaneously, a Faraday cup is set in the primary beam.

An on-line computer controls and actuates all the elements of the spectrometer : magnets, slits and beam diagnostics. The main characteristics of the line are given in table 1.

II.2 - Beam diagnostics - Intensity measurements

The primary beam intensity can be measured at several places of interest using Faraday cups or with a non-destructive intensity transformator.

The spatial distribution of such relatively intense beams can be

measured using multiwire secondary emission monitors. On the other hand, low intensity secondary beams are monitored by Ar-Co_2 filled multiwire proportional chambers operating either as ionisation chamber ($\simeq 10^3$pps) or as proportional counters (down to 10^3pps). They have been calibrated using an α radioactive source to give absolute intensities for a given gaz pressure and composition, and for various applied voltages [4].

II.3 - Energy degrader as a selection tool

An energy degrader, installed in the dispersive focal plane performs a supplementary selection in $Z^{1.5}/A^{2.5}$ due to a differential slowing down provided in the degrader. Moreover, the degrader used must be of variable thickness in order to compensate the energy spread and preserve the optical properties of LISE. Tuning the second dipole for some selected nuclei, four or five nuclei are focused in the focal point. An example of the selectivity due to a thick energy degrader is shown in fig. 2. This powerful method, essential for production of secondary beam, with a high purity [5,6], is also currently used by the Bordeaux-GANIL collaboration [7,8,9] which operates LISE as a Projectile Fragmentation Isotope Separator (P.F.I.S) for spectroscopic decay studies of exotic nuclei.

II.4 Thin position sensitive detector to improve the Mass resolution

A parallel plate avalanche counter (PPAC) [3] can be placed in the intermediate focal plane of the first dipole and gives a very good determination of the position of the nuclei trajectory, at this point (i.e. $B\rho$ determination). An excellent A-resolution ($\Delta A/A = 0{,}45\%$ at $A = 37$ for a slit aperture of ± 50 mm) is obtained, as it is shown in fig. 3.

II.5 - Sextupole to improve the beam size at the intermediate focal plane

The intermediate dispersive focal plane, actually, has a slope of only 20° compared to the beam axis. This slope increases the beam size and, thus, degrades the separation at this location. A sextupole will be placed at the intermediate focal plane. It must set upright the focal (more than 70° compared to the beam axis) and improve the separation [10].

III - SOME EXPERIMENTAL RESULTS

A projectile-like fragmentation process, in the intermediate energy domain, can produce nuclei far from the stability. These products are moving close to the projectile velocity and are strongly foward emitted [11]. The LISE spectrometer is evidently well-suited to collect new exotic nuclei produced with these above properties.

Secondary beams, as well as the study of new exotic nuclei need a good choice of target, projectile and beam energy to optimize the production rate. This choice can be done, with a good accuracy, using a simple abrasion-ablation model combined with a deexcitation stage of the primary distribution [11,12].

III.1 - Secondary radioactive beams

For the fragments rather close to the projectile mass, the LISE spectrometer can deliver radioactive beams with a good energy resolution and a small amount of contamination [5,6]. The yields I/Io (secondary/primary beams intensity) obtained with 44 MeV/u ^{40}Ar and 65 MeV/u, ^{18}O MeV/u are summarized in table 2.

A high beam purification is obtained by :

- choosing the right target thickness and nature : Be targets are more efficient by a factor 2.5 relative to Al and 5 relative to Ni targets, in a comparable situation, for the production of secondary beams which have a mass close to the projectile one.
- reducing the $B\rho$ acceptance of the line (i.e. of the slit aperture) in order to better separate the isotopes in ΔE-E plot (see fig. 4)
- adjusting the $B\rho$ value (see fig. 5)
- placing a thick energy degrader in the intermediate focal plane and by tuning the magnetic field in the second dipole to keep the achromatism of the line (see fig. 6).

III.2 - Production and identification of new proton rich nuclei.

Identification technics

For the identification of the produced fragments, the detection system consists of a standard solid state detector telescope (300μ,1000μ, 1000μ, 4000μ) placed at the focal final plane of LISE. The time of flight (T.O.F) of the detected fragments is measured between the target and this telescope (18 m) by deriving signals from the ΔE detectors and radiofrequency (R.F) of the last cyclotron : combined pieces of information from the telescope, the time of flight and the magnetic rigidity ensure an overdetermined identification of the fragment mass A and atomic number Z.

The particle identification is unambiguously achieved when looking at the bidimensional plot (see fig. 7) of $\sqrt{\Delta E}$/T.O.F. (i.e. Z) versus time of flight (i.e. A/Z). It exhibits characteristic curves which are related to a given isospin projection T_z. The line of constant T.O.F., corresponding to T_z=0 N=Z self conjugate nuclei, correlates with the

absence of well known unbound nuclei ^{8}Be (T_z=0), ^{23} (T_z=-½) and ^{16}F (T_z=-1) readily assures the Z and A calibrations.

New proton rich nuclei

The series of the T_z =-5/2 nuclei (^{23}Si, ^{27}S, ^{31}Ar and ^{35}Ca) predicted to give the limits of the proton drip line has been experimentally seen [13] (^{35}Ca was firstly identified by its β-delayed 2p activity [22]. With the possible exception of ^{22}Si, one may assume the proton drip line, predicted by the mass formula of Garvey-Kelson, to be mapped experimentally up to Z = 20.

The proton-rich projectile ^{58}Ni (55 MeV/u) beam has been used to investigate the proton drip line towards higher atomic numbers. Two targets Ni (92 mg/cm^2) and ^{27}Al (60.4 mg/cm^2) have been bombarded.

Results indicate the bound character of ^{43}V, ^{44}Cr $^{46-47}Mn$, (see fig. 8) and ^{48}Fe, $^{50-52}Co$, $^{51-52}Ni$ $^{55-56}Cu$ (see Fig. 9). The observation of these new Cu isotopes would demonstrate clearly that, at the intermediate energy domain, not only the projectile fragmentation process, but also transfer reactions produce new exotic nuclei. For the odd elements Z = 23, 25, 27, 29 : these results are in agreement with the predicted position of the drip line calculated by the charge formula of Garvey and Kelson [14], as done by Janecke [15] using the most recent experimental masses [16] but one must be cautious before making definite statement on whether or not the drip line has been reached for these odd isotopes, owing to the steepness of the valley of β stability on the proton rich side.

IV - CONCLUSION

All the new exotic nuclei [13, 17, 18, 19], half-lives and level schemes [7, 8, 9] determined at LISE and the results concerning the mass measurements performed at SPEG [20] are summarized in fig. 10. This progress, in the exotic nuclei domain is due to the various and high-intensity beams available at GANIL combined with the properties of the projectile-like fragmentation and with the good performances of the spectrometer.

Acknowledgements

I am grateful to all my colleagues from GANIL and ORSAY for initiating myself into the exotic physics. Special thanks are due to D. Guillemaud-Mueller, R. Anne and D. Guerreau for a critical reading of the manuscript and to R. Bimbot for enlightening discussions on secondary beam production.

Table 1 : Characteristics of the LISE beam line

Solid angle	Ω = 1 msr
Maximum rigidity	$B\rho$ max = 3.2 Tm
Dipole deflection angle	$\Theta = 45°$
Central trajectory radius	ρ = 2 m
Dispersion in focal plane	$D = \Delta x/100(\Delta B\rho/B\rho)$ = 18 mm
Maximum slit aperture	$S_{max} = \pm$ 50 mm
Corresponding maximum $B\rho$ acceptance	$(\frac{\Delta B\rho}{B\rho}) = \pm 2.717\%$
Total distance from target to achromatic focal point	L = 18 m

Table 2 : Production yields (I/I. for various secondary beams (S.B.) obtained from ^{40}Ar and ^{18}O primary beams.

Primary beam	Target	S.B.	I/I_0	S.B.	I/I_0	S.B.	I/I_0
44 MeV/u ^{40}Ar	99 mg/cm^2 Be	^{41}K	5.10^{-5}	^{38}Ar ^{39}Ar	10^{-4} 3.10^{-4}	^{39}Cl ^{38}S	10^{-4} $0.6.10^{-5}$
65 MeV/u ^{18}O	567mg/cm^2 Be	^{18}N ^{17}N	2.10^{-6} $\sim 10^{-4}$	^{16}C ^{15}C	2.10^{-6} 4.10^{-6}	^{13}B ^{12}B	$1.5.10^{-6}$ 10^{-6}
65 MeV/u ^{18}O	1026mg/cm^2 Be	^{17}N	5.10^{-6}	^{16}C	$0.5.10^{-6}$		

FIGURE CAPTIONS

Figure 1 Experimental set up : the LISE beam line.
The symbols q_1 to q_4, and Q_1 to Q_{10} refer to quadrupoles, D_1, D_2 to dipoles. The target is denoted by T, the slits by S, the achromatic focal point by F, and the telescope by TEL. Faraday cups are placed at points I, II, IV, V, and beam diagnostics (secondary emission and ionization chambers) at points I, II, III, IV and V.

Figure 2 Bidimensional plot of time of flight versus Z obtained in the ^{40}Ca (77 MeV/u) + Ni collision
a) without energy degrader at $B\rho = 2.10$ Tm
b) with a thick energy degrader (295 mg/cm^2) and the value of $B\rho_1 = 2.10$ Tm ; $B\rho_2 = 1.70$ Tm.

Figure 3 Mass histograms of phosphorus isotopes a) using the $B\rho$ value obtained with a parallel plate avalanche counter ($\Delta A/A = 0.45\%$ for A = 37) b) calculated with the following parameters : the total energy E_{tot} and the time of flight T.O.F. determined from the time signal of the ΔE detector and the radio frequency (R.F.) signal of the last cyclotron ($\Delta A/A \sim 0.6\%$ for A = 37).

Figure 4 Beam purity measurements obtained for a 99 mg/cm^2 Be target, and $B\rho = 1.938$ Tm
4a) Bidimensional plot E-ΔE for a slit aperture of $\pm$ 25 mm ($\Delta B\rho/B\rho = \pm 1.4\%$)
4b) Same as fig. 4a for a slit aperture of $\pm$ 5 mm ($\Delta B\rho/B\rho = 0.28\%$)

Figure 5 Effect of a B_ρ variation on the ^{39}Cl secondary beam purity. The beam compositions are shown for 5 different B_ρ values (in Tm). The ordinate scales correspond to arbitrary units. The B_ρ value of 1.972 Tm gives the best purity (84%) for ^{39}Cl secondary beam ; the main contaminants ^{40}Cl (4%), ^{36}S(4,5%) and ^{37}S (3%) are indicated close to the corresponding peaks.

Figure 6 Bidimensional plot showing the isotopic composition of a secondary beam obtained in the following conditions :
65 MeV/u ^{18}O + 1036 mg/cm^2 Be ;
a) unpurified beam (B_{1_ρ} = 2.248 Tm, $\Delta B\rho/B\rho = \pm$ 0.22%)
b) ^{16}C purified beam (B_{1_ρ} = 2.248 Tm, 150 mg/cm^2 Al intermediate degrader, B_{2_ρ} = 2.114 Tm, $\Delta B\rho/B\rho = \pm$ 2.78%)

Figure 7 A bidimensional plot of Z versus time of flight (see also text)

Figure 8 Mass-distributions for the elements V, Cr and Mn. They have been obtained by summing up the data at different magnetic rigidity setting : $B\rho$ = 1.80, 1.85 and 1.90 Tm. Thus, 181, 9, 334 and 15 events are observed for ^{43}V, ^{44}Cr, $^{46-47}Mn$ respectively.

Figure 9 Mass distributions for the elements : Fe, Co, Ni ($B\rho$ = 1.80, 1.85 and 1.90 Tm) and Cu ($B\rho$ = 1.90 and 1.95 Tm). Thus 27, 36, 442, 3232, 7, 68, 49, 380 events are observed for ^{48}Fe, $^{50-51-52}Co$, $^{51-52}Ni$ and $^{55-56}Ni$.

Figure 10 Summary of experimental measurements performed at GANIL : the bound character of new isotopes, half-lives and mass measurements are indicated respectively by stars, points and squares. The calculated drip lines are also shown by a solid line as predicted by Uno-Yamada [21] for neutron rich side and Garvey-Kelson formulae [14, 16] for the proton rich side. Nuclei predicted to be unbound against 1p and 2p emission are represented in dotted lines. The thick lines refer to the last known isotope on both the neutron rich and the proton rich sides.

REFERENCES

1 - ANNE R., SIGNARBIEUX C. ; GANIL report RA/NJ 278/82 (1982).

2 - LANGEVIN M., ANNE R. ; Proceedings of the conference on instrumentation for Heavy Ion Nuclear Research, Oak Ridge, Tennessee, oct.22-24 (1984) GANIL report 84.16 (1984).

3 - ANNE R., BAZIN D., JACMART J.C., LANGEVIN M., MUELLER A.C. ; To be published in N.I.M.

4 - BAZIN D., BOUVERET Y. ; GANIL report R.S 84-03.

5 - BIMBOT R., DELLA NEGRA S., AGUER P., BASTIN G., ANNE R., DELAGRANGE H., and HUBERT F. ; Z. Physik A322 (1985) 443.

6 - BIMBOT R., Invited talk presented at the International Conference on Heavy Ion Nuclear Collisions in the Fermi Energy Domain. Caen May 1986.

7 - HUBERT F. ; Invited talk presented at the International Conference on Heavy Ion Nuclear Collisions in the Fermi Energy Domain, Caen May 1986

8 - DUFOUR J.P., DEL MORAL R., EMMERMANN H. , HUBERT F., JEAN D., POINOT C., PRAVIKOFF M.S.,FLEURY A., DELAGRANGE H., SCHMIDT K.-H. ; Nucl. Inst. Method (in press).

9 - DUFOUR J.P., DEL MORAL R., FLEURY A., HUBERT F., JEAN D., PRAVIKOFF M.S., DELAGRANGE H., GEISSEL H., SCHMIDT K-H, to be published in Z. Physik.

10 - BAZIN D. ; GANIL report R.S 85.03.

11 - GUERREAU D. ; Invited talk presented at the International Conference on Heavy Ion Nuclear Collisions in the Fermi Energy Domain, Caen May 1986.

12 - GUERREAU D. ; to be published.

13 - LANGEVIN M., MUELLER A.C., GUILLEMAUD-MUELLER D., SAINT LAURENT M.G., ANNE R., BERNAS M., GALIN J., GUERREAU D., JACMART J.C., HOATH S.D., NAULIN F., POUGHEON F., QUINIOU E. and DETRAZ C. ; Nucl. Phys. A455 (1986) 149-157.

14 - KELSON I. and GARVEY G.T. ; Phys. Lett. 23 (1966) 689.

15 - At Data and Nucl. Data Tables 17 (1976), S. Maripuu special editor

16 - WAPSTRA A.H. and AUDI G. ; Nucl. Phys. A432 (1985) 1.

17 - LANGEVIN M., QUINIOU E., BERNAS M., GALIN J., JACMART J.C., NAULIN F., POUGHEON F., ANNE R., DETRAZ C., GUERREAU D., GUILLEMAUD-MUELLER D. and MUELLER A.C. ; Phys. Lett. 150B (1985) 71

18 - GUILLEMAUD-MUELLER D., MUELLER A.C., GUERREAU D., POUGHEON F., ANNE R, BERNAS M., GALIN J., JACMART J.C., LANGEVIN M., NAULIN F., QUINIOU E. and DETRAZ C. ; Z. Physik A322 (1985) 515

19 - POUGHEON F., GUILLEMAUD-MUELLER D., QUINIOU E., SAINT-LAURENT M.G., ANNE R., BAZIN D., BERNAS M., GUERREAU D., JACMART J.C., HOATH S.D., MUELLER A.C. and DETRAZ C. ; Orsay preprint IPNO-DRE 86-05 ; to be published

20 - GILLIBERT A., BIANCHI L., CONSOLO A., FERNANDEZ B., FOTI A., GASTEBOIS J., GREGOIRE C.,MITTIG W., PEGHAIRE A., SCHUTZ Y., STEPHAN STEPHAN C., GANIL preprint P. 86-16 to be published in Phys. Lett. B and GILLIBERT A... to be published.

21 - UNO M. and YAMADA M. ; INS report NUMA 40 (1982)

22 - AYSTO J., MOLTZ D.M., XU X.J., REIFF J.E. and CERNY J. ; Phys. Rev. Lett. 55 (1985) 1384

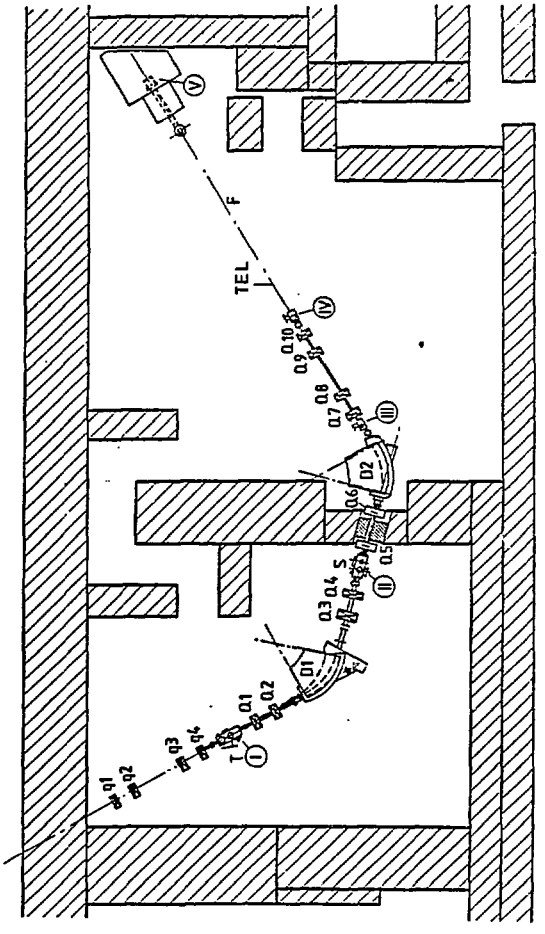

Figure 1

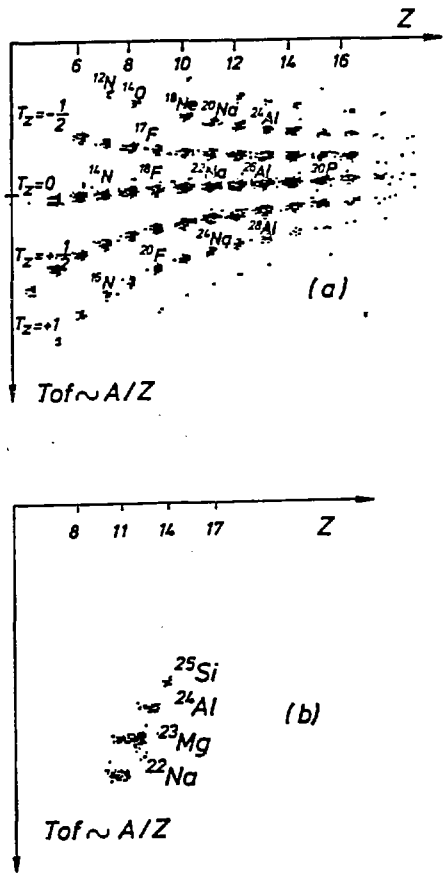
Z
6
8
10
12
14
16
^{12}N
^{14}O
^{18}Ne
^{20}Na
^{24}Al
$T_z=-\frac{1}{2}$
^{17}F
$T_z=0$
^{14}N
^{18}F
^{22}Na
^{26}Al
^{20}P
^{28}Al
^{24}Na
$T_z=+\frac{1}{2}$
^{20}F
^{16}N
(a)
$T_z=+1$
Tof ~ A/Z
8
11
14
17
Z
^{25}Si
^{24}Al
(b)
^{23}Mg
^{22}Na
Tof ~ A/Z

Figure 2

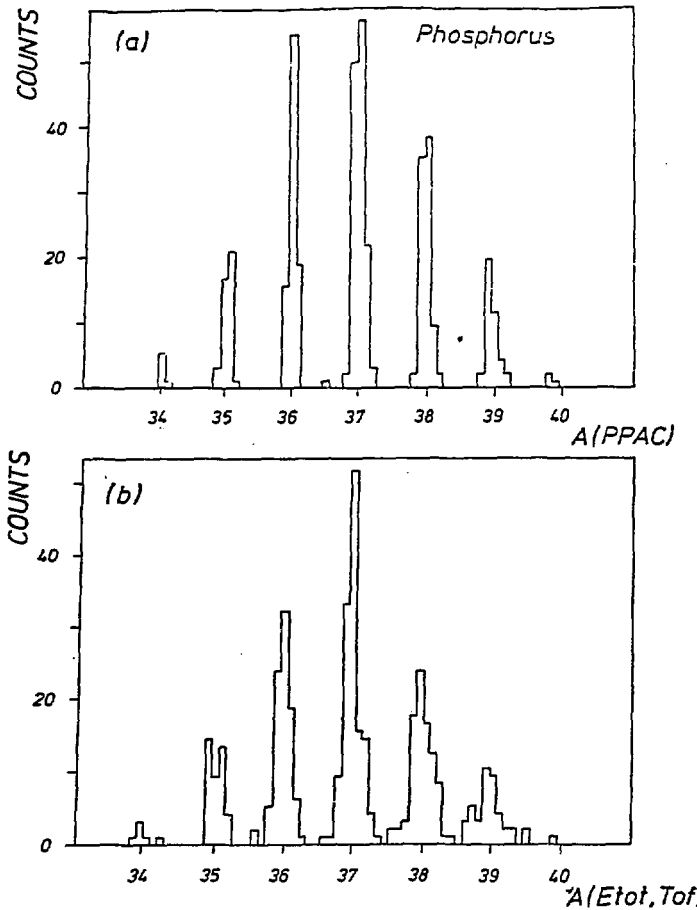
(a)
Phosphorus
COUNTS
40
20
0
34
35
36
37
38
39
40
A(PPAC)
(b)
COUNTS
40
20
0
34
35
36
37
38
39
40
A(Etot, Tof)

Figure 3

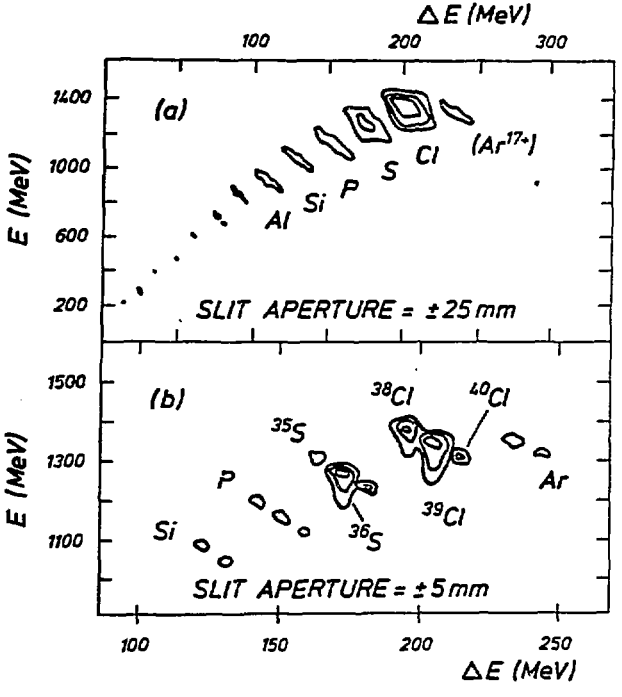
ΔE (MeV)
100
200
300
1400
1000
600
200
E (MeV)
(a)
Al
Si
P
S
Cl
(Ar17+)
SLIT APERTURE = ±25 mm
1500
1300
1100
(b)
35S
38Cl
40Cl
P
Si
36S
39Cl
Ar
SLIT APERTURE = ±5 mm
100
150
200
250
ΔE (MeV)

Figure 4

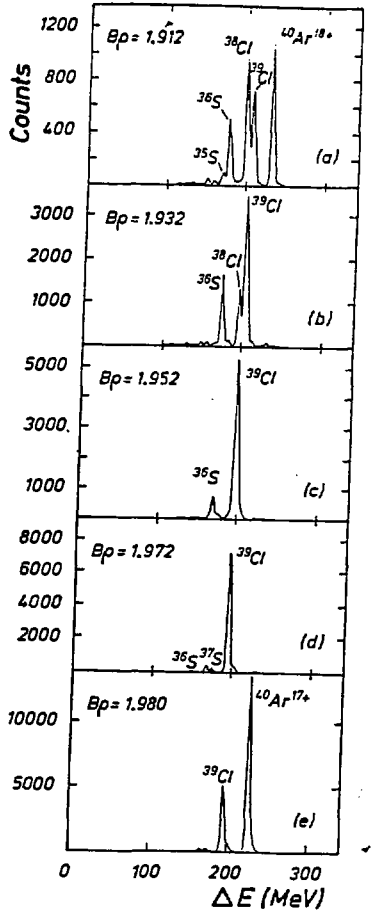
Counts
1200
800
400
Bρ = 1.912
38Cl
40Ar18+
39Cl
36S
35S
(a)
3000
2000
1000
Bρ = 1.932
39Cl
38Cl
36S
(b)
5000
3000
1000
Bρ = 1.952
39Cl
36S
(c)
8000
6000
4000
2000
Bρ = 1.972
39Cl
36S
37S
(d)
10000
5000
Bρ = 1.980
40Ar17+
39Cl
(e)
0
100
200
300
ΔE (MeV)

Figure 5

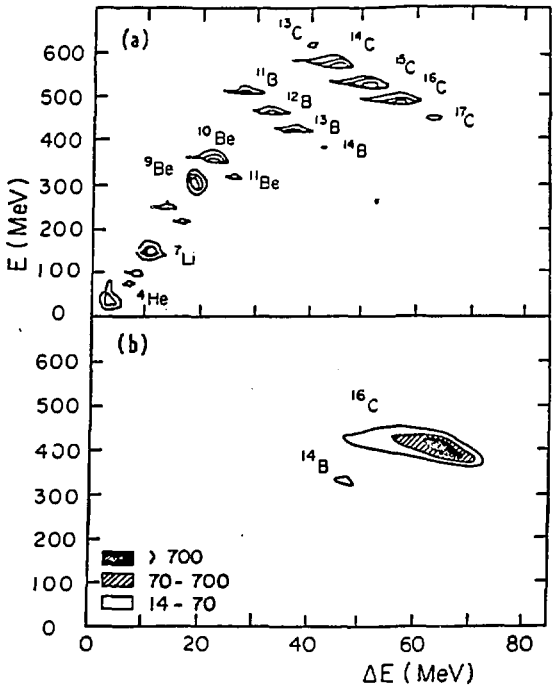
(a)
(b)
E (MeV)
ΔE (MeV)
0
100
200
300
400
500
600
0
20
40
60
80
^{4}He
^{7}Li
^{9}Be
^{10}Be
^{11}Be
^{11}B
^{12}B
^{13}B
^{14}B
^{13}C
^{14}C
^{15}C
^{16}C
^{17}C
> 700
70 - 700
14 - 70

Figure 6

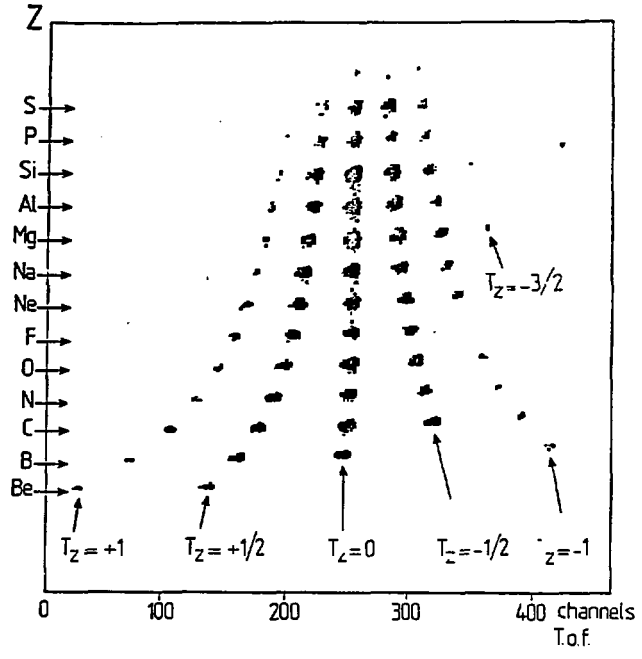
Z
S
P
Si
Al
Mg
Na
Ne
F
O
N
C
B
Be
$T_z = +1$
$T_z = +1/2$
$T_z = 0$
$T_z = -1/2$
$T_z = -1$
$T_z = -3/2$
0
100
200
300
400 channels
T.o.f.

Figure 7

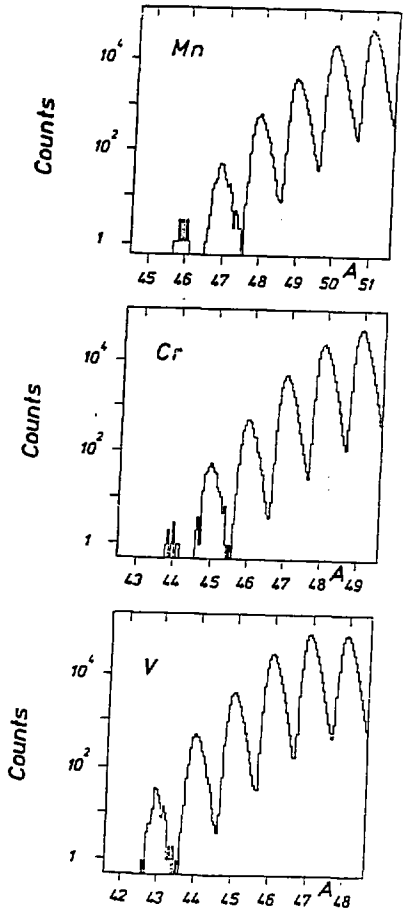
Mn
Cr
V
Counts
10⁴
10²
1
45 46 47 48 49 50 A 51
43 44 45 46 47 48 A 49
42 43 44 45 46 47 A 48

Figure 8

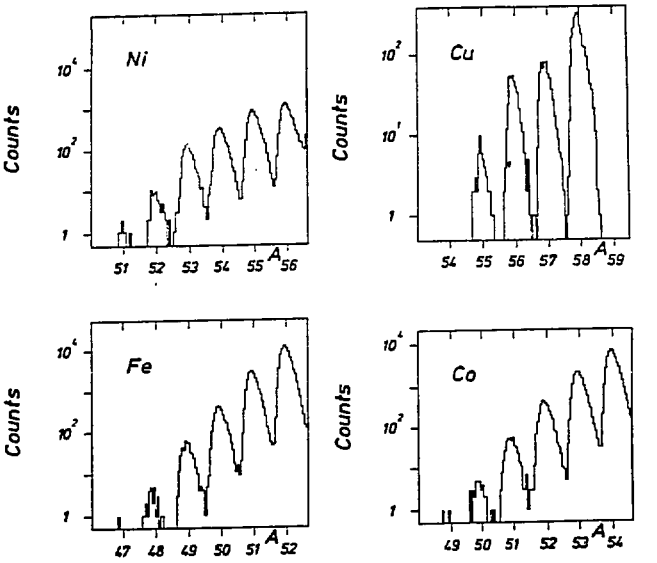
Ni
Counts
10⁴
10²
1
51 52 53 54 55 A 56
Cu
Counts
10²
10¹
1
54 55 56 57 58 A 59
Fe
Counts
10⁴
10²
1
47 48 49 50 51 A 52
Co
Counts
10⁴
10²
1
49 50 51 52 53 A 54

Figure 9

Figure 10